Engineered Science
DOI: https://dx.doi.org/10.30919/es986

Ambient Temperature Synthesis of Ultraviolet Emissive Carbon Quantum Dots from Kakadu Plum

Jamaan E. Alassafi[1,*] Yas Al-Hadeethi,[1, 2] Mohammed Saleh Aida,[1] Samar Fayez Al-Shehri[1] and Mingguang Chen[3]

Abstract

We proposed for the first time an efficient, environmentally friendly and energy-saving method for synthesizing carbon quantum dots at room temperature (RT.C-QDs). The Kakadu plum powder was used as a sole precursor without the use of external energy sources and chemical oxidants. The systematic analysis of as-synthesized RT.C-QDs reveals that they are composed of highly crystalline carbon quantum dots with an average diameter of 3.9 nm and exhibit an excitation-dependent emission characteristic with a quantum yield of 8.5%. The emission peak of RT.C-QDs was in a UV region at wavelength of 325 nm with high-color purity of narrow full width at half maximum (FWHM) at 50 nm, which is considered among the narrowest FWHMs reported to date. The obtained RT.C-QDs showed remarkable properties, including a unique graphitic carbon core encapsulated in an oxygen-rich amorphous shell, excellent water solubility, photostability, and environmental (pH) stability. This achievement could have significant implications for sterilization and photocuring applications and provide a promising direction for the development of practical and industrial ambient-temperature fabrication of carbon quantum dots.

Keywords: Ultraviolet; Carbon quantum dots; Narrow bandwidth; Ambient temperature synthesis; Kakadu plum powder.
Received: 03 August 2023; Revised: 04 October 2023; Accepted: 09 October 2023.
Article type: Research article.

1. Introduction

Fluorescence is an optical phenomenon that occurs frequently in nature, and related research is always under rapid development in both basic and practical applications. To date, several fluorescent materials such as inorganic quantum dots, small molecules, polymers and even rare-earth complexes have been designed and synthesized.[1-8]

Fluorescent carbon quantum dots emerge as a rising star in the last few years compared with traditional quantum dots due to their unique features such as excellent water solubility, outstanding photoluminescence (PL), low cost, high stability, low toxicity, good biocompatibility, and easy control of their physical and chemical properties.[9,10] In general, carbon quantum dots (C-QDs) are fluorescent carbon nanoparticles of spherical shape with an average diameter of less than 10 nm.[11] It is mainly composed of a graphitic core surrounded by an amorphous shell rich in functional groups.[12-14] Their outstanding optical properties are the result of the combination of the electronic properties of carbon nanoparticles with the unique optical properties of quantum dots. In other words, the quantum confinement effect governs the optical properties of C-QDs, and their emission wavelength can be tuned by controlling their sizes.

Since the discovery of C-QDs in 2004,[15] considerable progress has been achieved in research containing synthesis,[16-25] photoluminescence mechanism,[26-31] and applications.[32-35] To date, numerous efforts have been developed for the preparation of C-QDs by simple methods such as hydrothermal, pyrolysis, microwave plasma, and other techniques.[16-25] For example, Wang *et al*. report the production of multicolor C-QDs from ascorbic acid and phenylenediamine by hydrothermal method under reaction temperature at 160 °C for 6 hours.[36] By changing the precursor ratio, they produce C-QDs with different emission colors of blue, green and orange. In contrast, Dager and his colleague utilized an ultrafast synthesis technique known as microwave plasma-enhanced decomposition (MPED) at an

[1] *Department of Physics, Faculty of Sciences, King Abdulaziz University, Jeddah 21589, Kingdom of Saudi Arabia.*
[2] *Lithography in Devices Fabrication and Development Research Group, Deanship of Scientific Research, King Abdulaziz University, Jeddah 21589, Kingdom of Saudi Arabia.*
[3] *Department of Chemical and Environmental Engineering, University of California, Riverside 92521, USA.*
**Email:* jalassafi@stu.kau.edu.sa (J. E. Alassafi)

elevated temperature of approximately 800 °C and a short duration of 5 minutes to produce blue emissive C-QDs from fenugreek seeds.[37] Although these synthesis methods are simple and rapid, they required complicated experimental setups and high energy consumption for the carbonization processes and the improvement of C-QDs crystallinity.[38]

Alternatively, the fabrication of C-QDs at ambient temperature without the need for external power supply has gained significant attention in recent years due to the desire for a simple, environmentally friendly, and energy-efficient method.[39-44] At ambient conditions, C-QDs can be synthesized utilizing two conventional methodologies: adding chemical oxidants such as H_2O_2,[39] sulfuric acid and nitric acid[40] or a strong alkali such as concentrated potassium hydroxide and sodium hydroxide.[41] to the reaction system and use the heat released to induce dehydration and carbonization of carbon precursors. For example, Zhang *et al*. report the synthesis of green emissive carbon nanoparticles with a high quantum yield of 50% at room temperature by using sucrose as the carbon source and sulfuric acid as the oxidant agent.[42] Xiao and his coworkers reported the fabrication of multicolor carbon quantum dots at room temperature using PEG 400 as the carbon source and NaOH as the strong alkaline environment.[43] As a result, carbon dots with different emission colors blue, yellow, orange-red and red were obtained and used for Fe^{2+} detection.

Despite the benefits of low-energy preparation and avoidance of side reactions in the form of chemical defects, the time-consuming nature of the RT synthesis procedure and the environmental concerns raised by the use of chemical oxidants hinder its widespread use. Furthermore, the majority of reported C-QDs have an amorphous structure and highly crystalline C-QDs have rarely been reported.[44]

Up to now, various carbon sources ranging from natural green sources[45] to chemical products,[46] from small molecules to aromatic compounds[47] have been used to produce fluorescent C-QDs. Nevertheless, scientists have recently focused their efforts on converting the low-cost of natural green sources such as plants and their derivatives (leaves, seeds, and roots) into valuable products due to their advantages of renewable energy, environmentally friendly, and widespread use. For instance, walnut peel,[48] garlic,[49] papaya juice,[50] rice husk[51] highland barley,[52] and lychee seeds,[53] are examples of natural green sources that are being used in advanced applications such as biological imaging, sensors, drug delivery, and more.[54,55]

In recent years, there has been significant progress in the development of fluorescent C-QDs that emit multicolor, long-wavelength, and even pure white light.[2,22,56,57] However, ultraviolet-emitting C-QDs have rarely been reported, and most of them exhibit broad emission bands with FWHM greater than 60 nm, as shown in Figs. 1a and b (Appendix Table S(1)), which severely limits their possible uses in high-precision optics. Therefore, it is essential to fabricate ultraviolet-emitting C-QDs with high color purity and a narrow bandwidth of less than 60 nm from renewable green sources for advanced optical applications.

In this study, we present a novel, eco-friendly, and energy-efficient technique for the production of C-QDs with ultraviolet emission at room temperature (RT C-QDs) using Kakadu plum as a sole carbon precursor. Kakadu plums are abundant in vitamin C, sugars, and carbohydrates, which act as a carbon source for the synthesis of RT.C-QDs. The morphology, chemical composition, and optical properties of RT.C-QDs were comprehensively examined. The RT.C-QDs exhibit a small average size of 3.9 nm, featuring a highly crystalline core structure encapsulated within an amorphous shell layer enriched in oxygen and nitrogen-related functional groups. Interestingly, the emission of the RT.C-QDs is dependent on the excitation, with the maximum intensity observed at 325 nm, and demonstrate a remarkably narrow full width at half maximum (FWHM) of 50 nm, which is believed to be one of the narrowest FWHMs reported by green sources to date, Fig. 1b. The relative quantum yields (QY) was

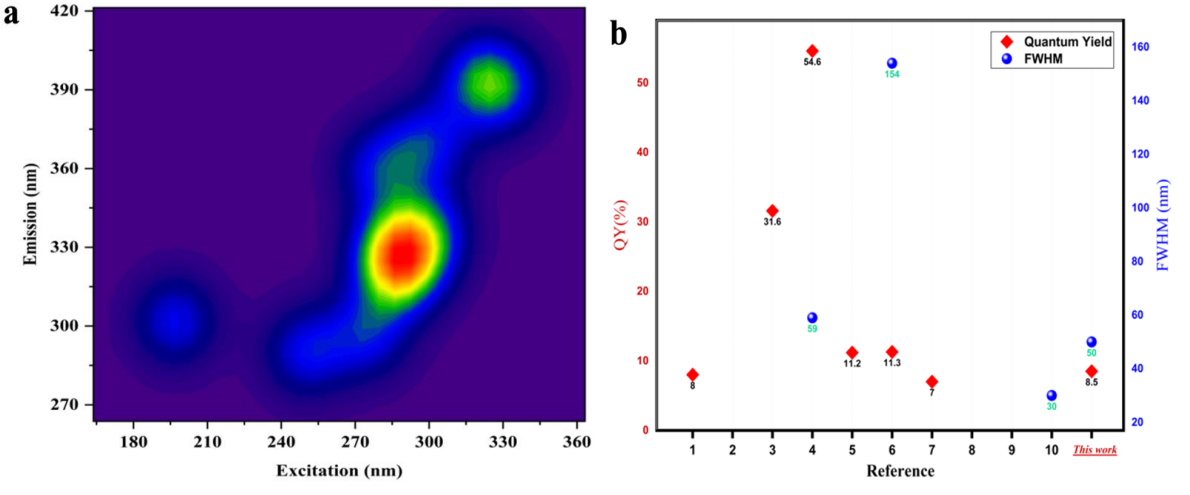

Fig. 1 (a) Excitation-emission map of recent reports on ultraviolet C-QDs, showing that most emit UV light at around 330 nm when excited at a wavelength of 285 nm. (b) the statistical distribution of the reported quantum yields and full width at half maximum (FWHM) of UV C-QDs, showing that our work is among the narrowest FWHM reported to date.

measured at 8.5% and showed high photostability and environmental stability (pH). This method provides a powerful strategy to fabricate highly crystalline C-QDs without using chemical oxidant agents and external energy supplies.

2. Experimental Section

2.1 Materials

Kakadu plum powder from (Australian SuperFood Co, Australia) was used in as-is form without any modification and purification. High-purity water was used throughout the experiment.

2.2 Synthesis of RT.C-QDs

Kakadu plum is a rich source of natural Vitamin C and it is widely used as a powerful antioxidant and immune-boosting superfood. To date and to the best of our knowledge, Kakadu plum powder has never been used as a source of carbon quantum dots (C-QDs).

Here, RT.C-QDs were fabricated in one simple step at room temperature without energy consumption or modification as shown in Fig. 2. First, 0.3 g of yellow powder of Kakadu plum was dissolved in 100 ml of ultrapure water in a glass beaker and stirred for 15 minutes. The resulting yellowish solution was filtered through a 0.22 µm syringe filter and centrifuged at 10,000 rpm for 30 minutes to remove the large unreacted particles. The filtered solution was then further purified using a dialysis kit (Float-A-Lyzer, 0.1-0.5 k Da). The obtained product was a colorless transparent solution that subjected to vacuum freeze-drying procedure for 3 days to obtain the desired powder of carbon dot. Then, the resulting powder was dissolved in ethanol and exhibited UV emission at 325 nm upon excitation with a wavelength of 290 nm. Finally, the RT.C-QDs solution was transferred to a glass vial and stored in the dark at room temperature for further characterization.

Figure 3 illustrates the formation steps of RT.C-QDs which consist of four main steps; dehydration, carbonization, functionalization and formation. The Kakadu plum powder is complex in nature since it is rich in photochemical and poly-hydroxyl species containing large numbers of carbons. Basically, it contains the highest vitamin C levels of all fruits in the world. Based on the fact sheet of nutrition information by the producer, 100 g of the freeze-dried powder of Kakadu plum contains 8.3 g of vitamin C, 3.3 g of saturated fat and 3.3 g of carbohydrate that serves as a carbon source. In addition, it contains 3.3 g of protein, which serves as both carbon and nitrogen sources.

First, the dehydration reaction takes place upon adding 0.3 g of the Kakadu plum powder to 100 ml of high purity water under constant stirring, where a colorless water turns into a yellowish solution due to the occurrence of n-π multiple electronic transitions of highly polar compounds such as OH, NH and C=O. This leads to a time-dependent leaching of the Kakadu plum powder in the water and as the reaction time progresses, more carbon molecules are dispersed. During this process, heat facilitates the removal of water molecules from ascorbic acid, leading to the formation of dehydrated ascorbic acid intermediates. This step can be represented by the equation:

Ascorbic Acid → (heat) Dehydrated Ascorbic Acid Intermediates + H_2O

After dehydration, the dehydrated ascorbic acid intermediates undergo carbonization, a thermal decomposition

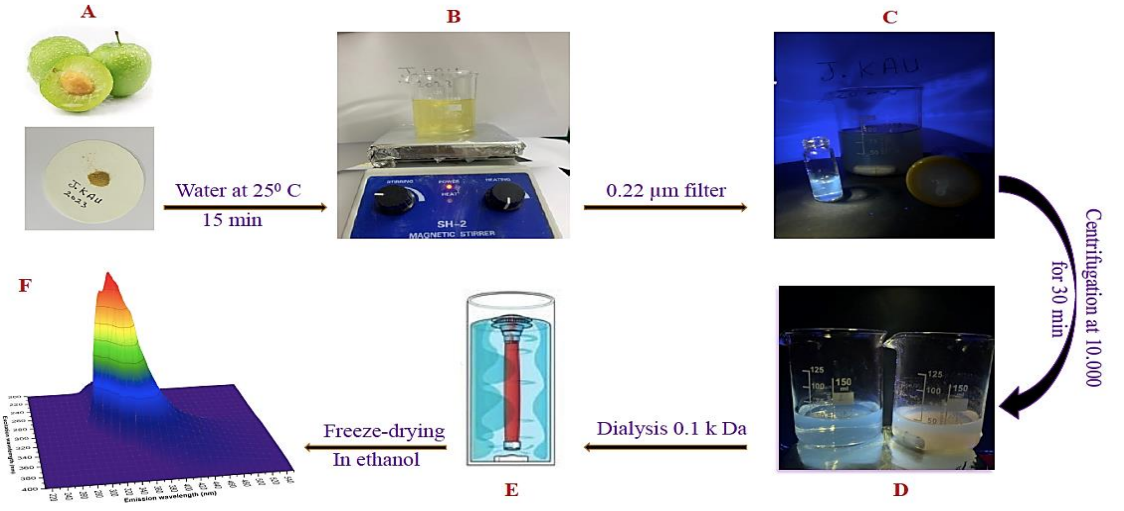

Fig. 2 Shows the experimental procedure for synthesizing RT.C-QDs using Kakadu plum powder. (a-c) The powder is dissolved in water and filtered to obtain a blue solution. (d) Centrifugation further enhances the blue color. (e) The solution is then dialyzed and (f) the resulting powder emits UV light at 325 nm when dissolved in ethanol.

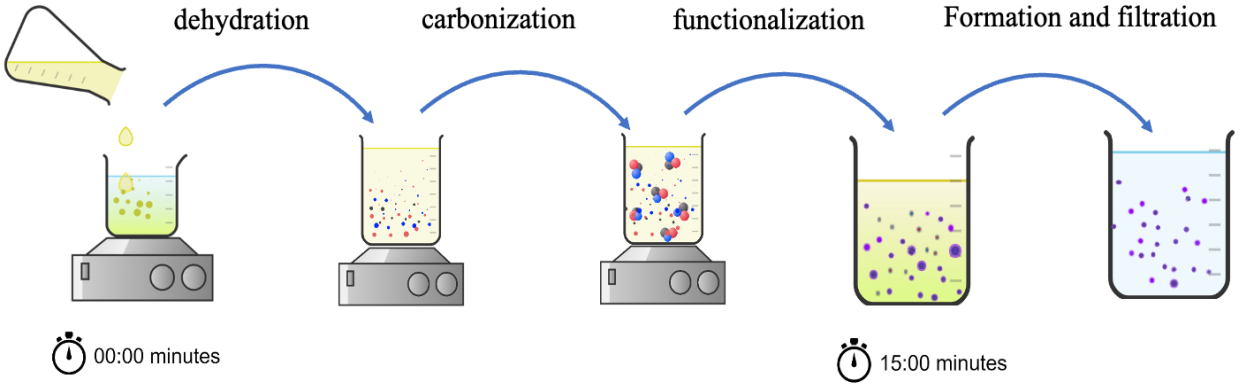

Fig. 3 The schematic figure shows the RT.C-QD synthesis from Kakadu plum powder at room temperature shows main formation steps of dehydration, carbonization, functionalization and formation.

process in which complex molecules break down into simpler carbon structures. As the reaction time progresses, the number of carbon molecules increases and the space between them becomes shorter until it reaches a critical point where the carbon species interact with each other to form smaller nuclei due to Van der Waals attractive forces. These smaller carbon nuclei continue to grow with the availability of additional carbon atoms to diffusely form the carbon core of the quantum dots (C-QDs) until no more carbon is available to contribute to the formation of new C-QDs. This formation of the carbon serves as the nucleus for the formation of room-temperature carbon quantum dots (RT.C-QDs), which can be represented as:

Dehydrated Ascorbic Acid Intermediates → (heat) Carbon Core + CO + CO_2

After carbonization, the carbon core undergoes functionalization, a crucial step in which oxygen and nitrogen-related functional groups (-OH, -COOH, NH_2, *etc*.) are introduced on the surface of the carbon core. This process, facilitated by the compounds present in the Kakadu plum extract, enhances the solubility and stability of the carbon quantum dots, making them suitable for various applications. It can be described as:

Carbon Core + Functionalizing Agents → Functionalized Carbon Quantum Dots

In the final step, UV-emitting centers are formed within the carbon quantum dots, which are responsible for their ultraviolet emission properties. This process could involve coordination or interaction with specific compounds present in the Kakadu plum extract that have UV emissive properties. The precise nature of these emissive centers is an area for further research and exploration. These UV-emitting C-QDs were effectively extracted from the solution through filtration and dialysis procedures, separating them from large unreacted particles that cause the reduction in emission intensity and broadening of emission peaks.

This detailed mechanism provides insights into the molecular transformations occurring during the synthesis of ultraviolet emissive carbon quantum dots from Kakadu plum powder. It offers a theoretical foundation for understanding the unique properties of these quantum dots and their potential.

2.3 Characterization of RT.C-QDs

2.3.1 The morphology and size distribution

The morphology and size of RT.C-QDs were investigated by a scanning electron microscope (SEM) model JSM-7600F (JEOL, Tokyo, Japan) and a high-resolution transmission electron microscope (HRTEM) model Jem-2100f operated at 200 kV (Jeol, Tokyo, Japan). The crystallinity structure was studied by using X-ray diffraction (XRD) on an Ultima-IV system with filtered Cu Kα radiation (λ = 1.54056 Å), and Raman analysis was performed using micro-Raman spectroscopy (Thermo, USA).

2.3.2 The surface chemical composition

The surface chemical composition of RT.C-QDs was studied by X-ray photoelectron spectroscopy (XPS) model (K-Alpha Plus, Thermo Fisher, United States) and FTIR (Thermo-Scientific, Waltham, MA, USA).

2.4 The photoluminescence mechanism and photostability

The photoluminescence emissions of the RT.C-QDs were investigated by using a fluorescence spectrophotometer F-7000 (Hitachi, Japan). Absorption spectra of RT.C-QDs were recorded by using a UV-Visible spectroscopy model Lambda 750 (PerkinElmer, Waltham, MA, USA). The photostability of RT.C-QDs was investigated by using Camag UV Cabinet II of 55 W UV source and wavelength of 250 nm for 60 minutes.

2.5 The Quantum Yield (QY) Measurement

A relative method was used to calculate the quantum yield (QY) of the RT.C-QDs. 2-Aminopyridine (QY=66% in 0.1 N H_2SO_4, excitation wavelength at 290 nm) was used as a reference standard because its absorption and emission wavelength are comparable to our sample.[58] The 2-Aminopyridine was dissolved in 0.1 N H_2SO_4 aqueous solution and the RT.C-Ds were dissolved in ethanol solution for the experiments. A series of reference solutions and RT.C-QDs were prepared with different concentrations ranging between 0 and 0.1. The photoluminescence spectra were

measured, and the photoluminescence intensity was integrated under the photoluminescence curve. The slope was calculated using the integrated emission intensity versus absorption plot. The QY of RT.C-Ds was then determined using the following equation:

$$\Phi_S = \Phi_R \times \frac{G_S}{G_R} \times \frac{\eta_S{}^2}{\eta_R{}^2} \quad (1)$$

where Φ, G and η are quantum yield, integrated fluorescence intensity and refractive index of the solvent (1.33 for H_2SO_4 and 1.36 for ethanol) respectively. The subscript *R* refers to the reference standard with known quantum yield and the terms with the subscript *S* indicate the synthesized RT.C-QDs.

3. Characterization results

3.1 SEM and XRD

The morphology and size distribution of RT.C-QDs were studied by SEM and the high-resolution TEM as shown in Fig. 4 and Fig. 5, respectively. On a silicon substrate, the SEM images reveal a small island of carbon nanoparticles with excellent dispersion and relatively uniform size. Their surface morphology was investigated by using Energy Dispersive Spectroscopy (EDS) analysis which reveals they were mainly made from carbon and oxygen. Here the EDS analysis technique was implemented to ensure that the RT.C-QDs on the TEM grid contained no residual foreign elements other than carbon and oxygen. HR-TEM images show a wide range of size distribution of well-depressed carbon nanoparticles of spherical shapes with a clear crystalline lattice structure of their core surrounded by an amorphous shell. For the precise size distribution measurements, more than one hundred (120 counts) nanoparticles were taken into account and found to exhibit a wide range distribution in their sizes between 2.2 and 13.2 nm with an average size of 3.9 ± 1.6 nm, m. The as-synthesized RT.C-QDs show that the carbon core is composed of multilayer of graphite-like structure that stacked over each other with lattice spacing ranging from 0.21 to 0.32 nm assigned to the graphite crystal structure (100) and (002) diffraction planes, respectively.[59]

X-ray powder diffraction (XRD) and Raman spectroscopy were used to verify the core structure and the quality of graphitic structure of the RT.C-QDs, respectively. The XRD is a unique technique that can effectively distinguish between the signals coming from the core and the surface, providing information only about the core structure of RT.C QDs. The carbon core can be either a pure graphite core (sp^2), a purely amorphous core (sp^3), or a ratio of both sp^2/sp^3. The XRD patterns in Fig. 6a show two diffraction peaks at 20° and 38° assigned to (002) and (100) that corresponding to an interlayer distance of 0.44 and 0.24 nm of low and high graphite structures, respectively. This complements the HR-TEM data and proves the co-existence of graphitic and low graphitic structure in the carbon core of RT.C-QDs.

Raman spectroscopy is a powerful and non-destructive method for characterizing carbon-based nanomaterials. In this context, the assessment of graphite structure is investigated by estimating the ordered and disordered phases in RT.C-QDs. The disordered phase (D-band) represents the presence of defects (disordered sp^3-hybridized carbon), while (G-band) represents the vibration of sp^2-hybridized carbon atoms in graphitic structure. The Raman spectrum depicted in Fig. 6b

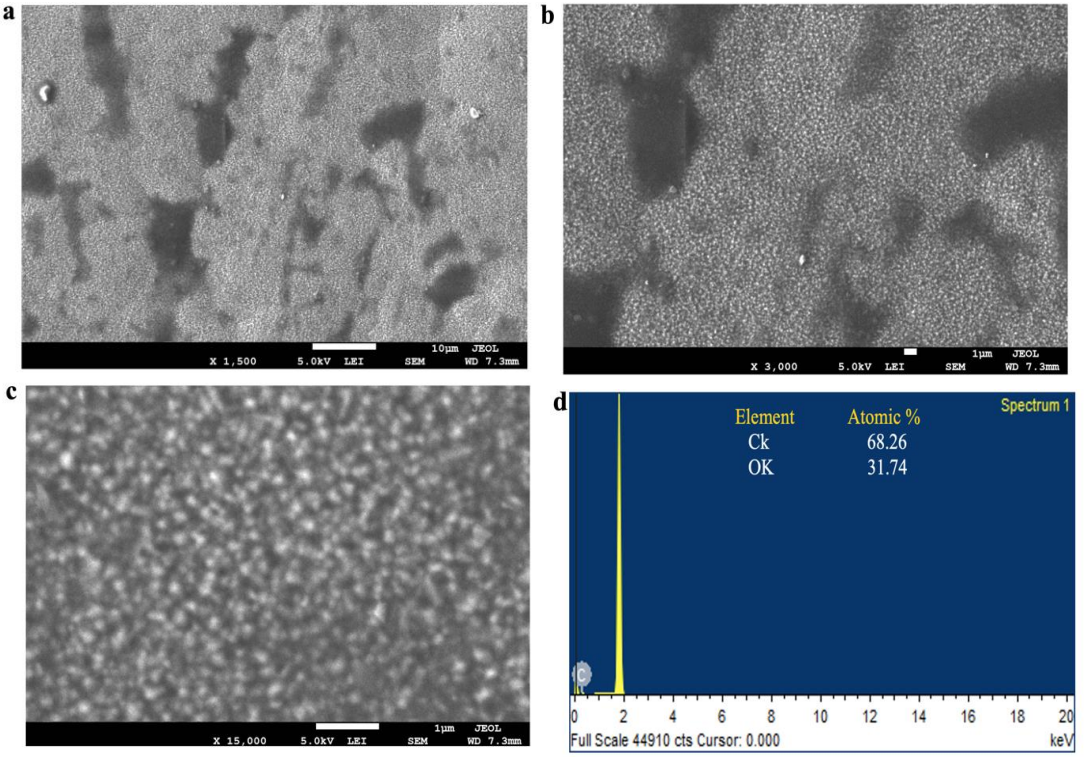

Fig. 4 (a, b and c) representative SEM images of RT.C-QDs that show a uniform distribution of carbon nanoparticles. (d) Energy Dispersive Spectroscopy (EDS) spectrum shows only carbon and oxygen elements on a silicon substrate.

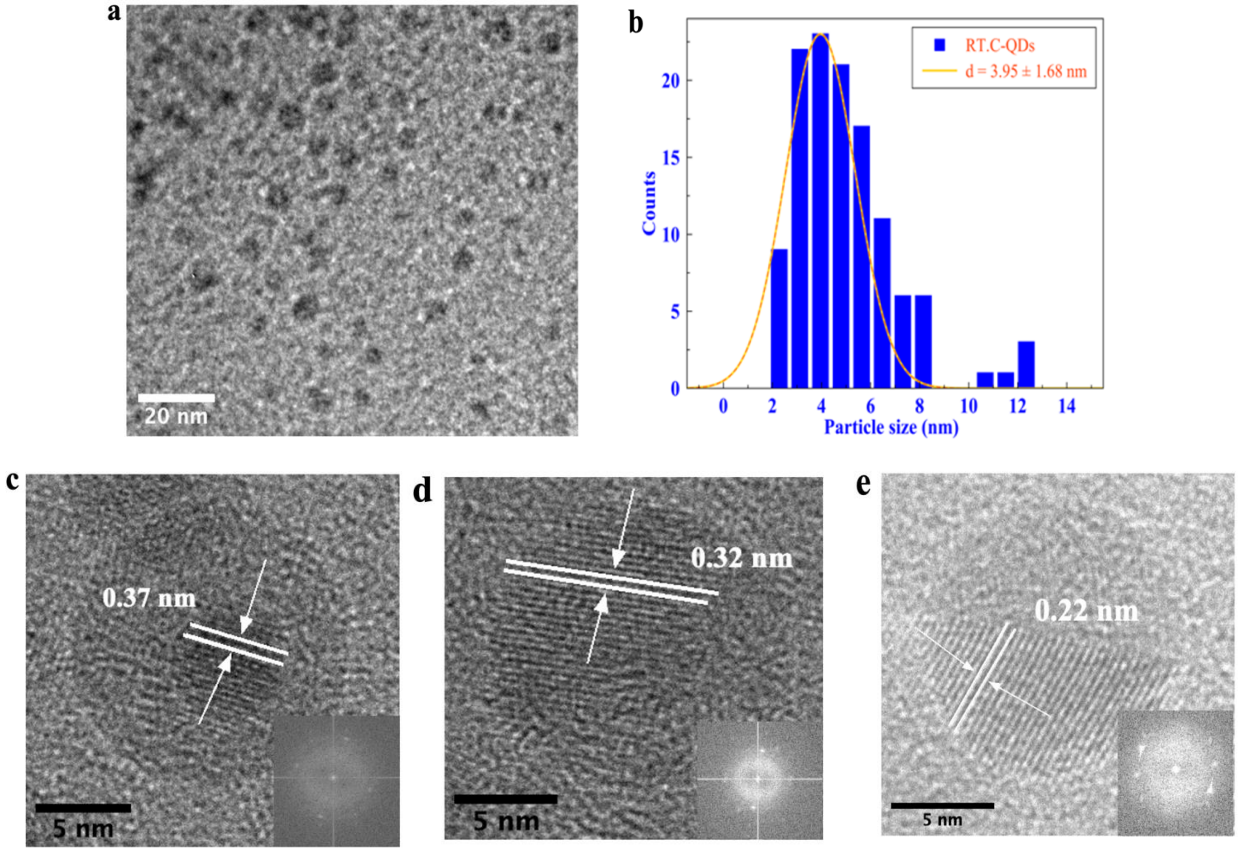

Fig. 5 (a) TEM image of RT.C-QDs (b) Histogram shows a wide range of particle size distribution. (c) RT.C-QDs at high resolution demonstrating a graphitic core structure inside amorphous shell layer. (d and e) demonstrating a d-spacing of graphitic structure ranging between 0.22 to 0.32 nm.

illustrates the distinct features of the disordered band (D) at 1372 cm^{-1} and the graphitic band (G) at 1590 cm^{-1}. The relative intensity ratio between the G and D bands (I_G/I_D) is determined to be 1.8, indicating the exceptional graphitic crystallinity exhibited by our prepared RT-C QDs. This observation is consistent with the results of HR-TEM, in which no amorphous structure was identified.

As confirmed by the data from HR-TEM, XRD, and Raman that reveal the RT.C-QDs have a crystalline core structure with negligible defects that distinguishes them from most reported amorphous carbon dots.[41,60,61]

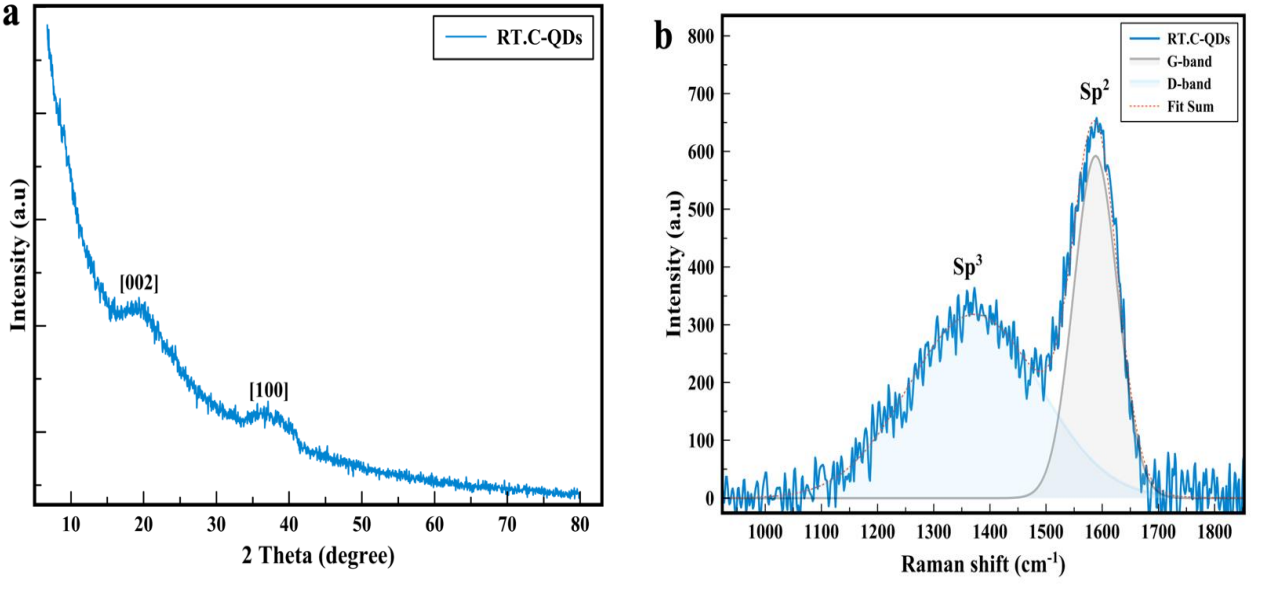

Fig. 6 (a) XRD pattern of the RT.C-QDs shows two diffraction peaks at 20° and 38°. (b) Raman spectra of the RT.C-QDs shows high graphitic crystallinity structure with relative intensity ration of G to D bands at 1.8.

3.2 Chemical composition

Chemical compositions and functional groups of the as-prepared RT.C-QDs were studied by X-ray photoelectron (XPS) and Fourier transforms infrared (FT-IR) spectroscopies. The XPS survey of RT.C-QDs is shown in Fig. 7a and reveals that the surface layer of the RT.C-QDs consists mainly of carbon (60.5 at.%), nitrogen (0.8 at.%) and oxygen (38.7 at.%). No other element was detected, indicating the high purity of the carbon precursor. The high-resolution spectra of C 1s, N 1s, and O 1s are shown in Figs. 7(c), (d), and (e), respectively. The C 1s peak can be deconvoluted into three peaks at 284.5 eV (22.1 at.%) corresponding to the sp^2 graphite structure C=C/C-C, while the dominant peak at 286.5 eV (57.3 at.%) assigned to the sp^3 of C-O/C-N. Another small peak at 288.3 eV (22.6 at.%) could be assigned to C=O/C=N. The high-resolution spectrum of N 1s can be deconvoluted into three peaks: pyridinic-N at 398.6 (37 at.%), pyrrolic N-H at 399.8 eV (46.3 at.%), and graphitic N-C at 401.2 (16.7 at.%), respectively. The high-resolution spectrum of O 1s can be deconvoluted into two peaks. The main peak is at 533 eV (58.9 at.%) and a minor peak at 531.5 eV (41.1 at.%), correspond to C-O and C=O, respectively.

FT-IR was used to get more insight into the chemical composition and functional groups on the surface layer of the RT.C-QDs as shown in Fig. 8. Obvious absorption peaks centered at 3310 cm^{-1} and 2921 cm^{-1} indicate the O-H/N-H bond and the symmetric CH_2, respectively. Stretching peaks at 1720, 1633, 1331 and 1030 cm^{-1} can be assigned to C=O, C=C, C-N, and C-O/C-H, respectively. Overall, the presence of a C=C peak suggests that the RT.C-QDs consist of a graphite structure surrounded on its surface by amorphous shells rich in OH, C=O, C-O/C-N, and C-H. Furthermore, the symmetrical CH_2 peak at 2921 cm^{-1} indicates that the hydrocarbon in the Kakadu plum powder is not fully carbonized and converted into graphitic carbon, which can be achieved by applying sufficient thermal energy.

3.3 Photostability and influence of pH on PL characteristics

The stability of C-QDs under ambient conditions is a prerequisite for their implementation in practical applications. For example, photostability is critical for applications exposed to light over a long period of time to ensure that their fluorescence intensity does not decay over time, whereas their stability over a wide pH range is crucial for sensing applications.

The high photostability of the synthesized RT.C-QD is shown in Fig. 9a. The photoluminescence intensity remains stable for 60 minutes after continuous irradiation with a 55 W xenon lamp at a wavelength of 250 nm, which could be attributed to their superior crystal structure and chemical stability.

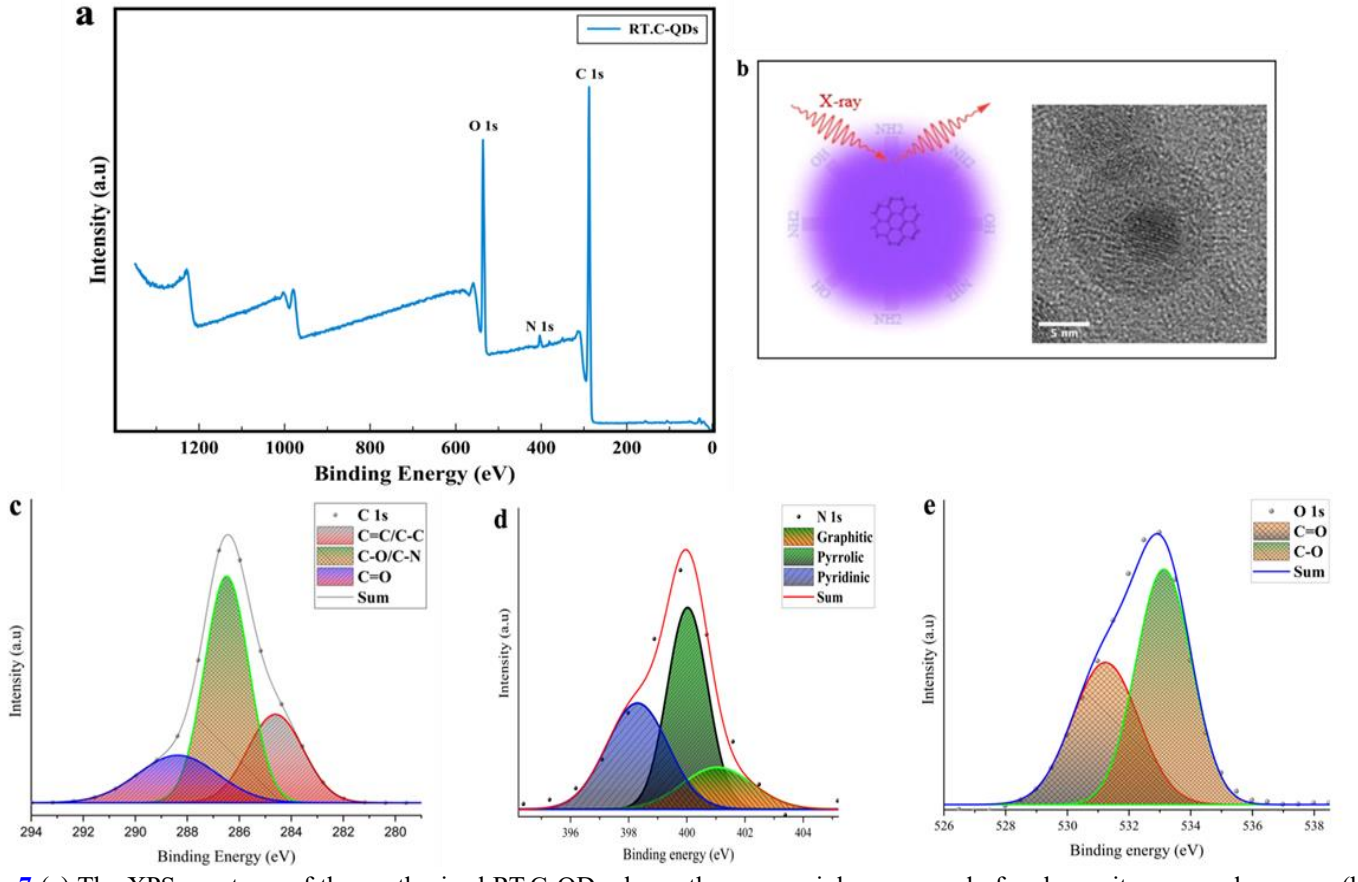

Fig. 7 (a) The XPS spectrum of the synthesized RT.C-QDs shows they are mainly composed of carbon, nitrogen, and oxygen. (b) schematic diagram of XPS characterization of the surface and a proposed structure of RT.C-QDs. (c) High-Resolution XPS of C 1s, (d) High-Resolution XPS of N 1s and (e) High-Resolution XPS of O 1s.

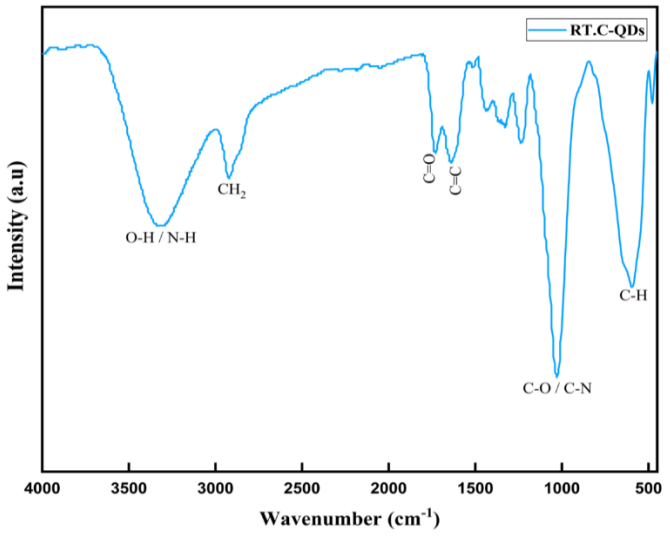

Fig. 8 FT-IR spectra of the RT.C-QDs shows their surface is rich with oxygen-related function groups.

The photoluminescence (PL) of RT.C-QD is sensitive to environmental factors such as pH and solvent type. Fig. 9b shows the photoluminescence of RT.C-QDs dispersed in ethanol at different pH values ranging from acidic at 5 to basic at 11. The PL of RT. C-QDs are independent of pH and have a broad emission peak position centered at 325 nm with a gradual increase in their intensity as pH changes from acidic to basic, consistent with the other reported.[62] The wavelength independence here indicates the limited involvement of surface states in changing the PL wavelength position and confirms the relatively low degree of functionalization and the well crystalline structure of RT.C-QDs.

4. Photoluminescence mechanism

The PL excitation-emission map of RT.C-QDs is presented in Fig. 10(a). The absorption, PL excitation, and emission spectra at room temperature are shown in Figs. 10(b), (c) and (d), respectively.

The PL excitation-emission map of RT.C-QDs shows excitation-dependent emission upon excitation with wavelengths ranging from 240 to 400 nm with a maximum emission intensity at 325 nm.

UV-Vis absorption spectroscopy reveals the presence of two absorption bands within the UV range, a high energy band from 200 to 290 nm, and a low energy band from 300 to 350 nm. At the high energy band, two peaks were observed. A minor peak at 225 nm and a dominant peak at 260 nm can be attributed to the π-π* transition of the carbon core (C=C). In addition, three peaks were also observed for the low energy band at 315, 325, and 350 nm, which can be ascribed to the n-π* transition of the surface containing oxygen and nitrogen related functional groups (C-O/C-N).[63-66] Besides these two bands, a long tail extending into the visible range of the spectrum can be ascribed to lower energy surface centers.[66,67] Similar to the UV-Vis results, the PLE spectra also reveal two distinct peaks. A small peak at 240 nm with a corresponding FWHM of 15 nm, and another dominant peak of maximum excitation intensity at 290 nm of FWHM at 19 nm, respectively. It is worth noticing that these two peaks could be related to the higher energy band of the absorption at 220 and 265 nm that is assigned to the carbon core, and the red-shift of about 25 nm reflects a non-radiative transition of electrons toward the emitting states.

The PL spectra of RT.C-QDs shows asymmetric emission peak at 325 nm and narrow bandwidth of FWHM at 50 nm when excited at wavelength at 290 nm. Clearly, there are at least two emissive centers that are active and constructed the main emission peak, which are a small peak at 311 nm (3.98 eV), and another larger peak with the highest intensity at 325 nm (3.81 eV). It can be noticed here that the difference between these two peaks, which was about 14 nm (0.17 eV) represents the difference in energy level between these two emissive centers.

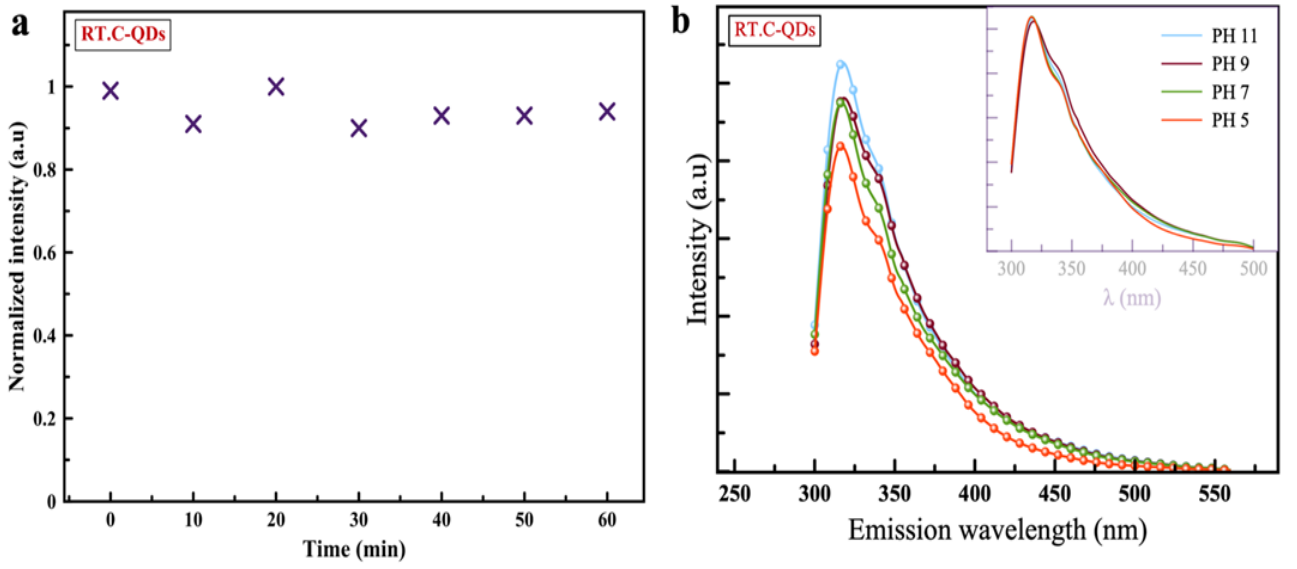

Fig. 9 (a) Photostability tests were performed at room temperature using a UV 250 nm with a 50 W xenon lamp for 60 minutes. (b) PL emission spectra of RT.C- QDs with different pH values at an excitation wavelength of 290 nm.

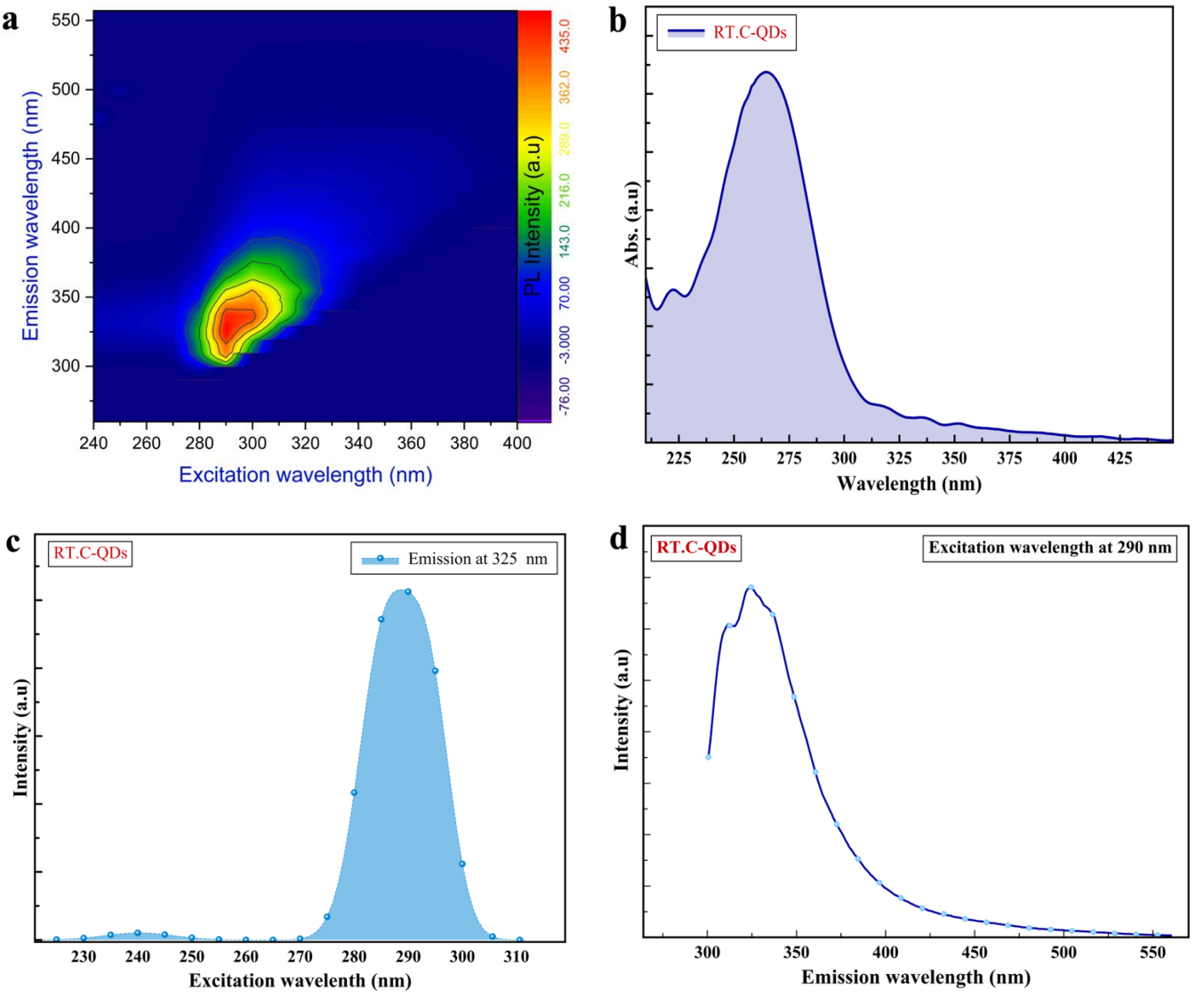

Fig. 10 Optical properties of RT.C-QDs in ethanol. (a) Excitation-emission color map. (b) optical absorption, (c) normalized PL excitation (290 nm), (d) and PL emission (325 nm).

Therefore, the absorption curve, PLE spectra, and emission curve all suggested the overall emission of our RT.C-QDs mainly originated from multi-type electronic transitions.

The origin of the photoluminescence (PL) mechanism of C-QDs is still debatable and a universal mechanism does not exist.[28,68] In general, the most acceptable PL mechanisms involve excitation-independent and excitation-dependent emission features.[68] The excitation-independent emission can be explained by a single electronic transition upon changing the excitation wavelength, which could be related to the presence of fluorophores[69] and the fully passivated ultra-small RT.C-QDs.[63] On the contrary, quantum confinement, heteroatom electronegativity, and surface trapping have been proposed to explain excitation-dependent emission, in which the emission peaks shift toward longer wavelengths with a gradual decrease in their intensities when excited at longer wavelengths.[70]

Figures 11a and 11b show the PL and PLE spectra of RT.C-QDs that exhibited an excitation-dependent emission property. The PL spectrum of RT.C-QDs show asymmetric emission peaks ranging from 300 to 550 nm, with the emission red-shifting to lower energy as excitation wavelengths changed from 280 to 400 nm. The emission intensities first increased with increasing excitation wavelengths reaching their maximum at 325 nm and then gradually decreased toward longer wavelengths. In addition, the PLE spectrum showed the contribution of the excitation wavelength at 290 nm to the overall emission with its maximum at emission wavelength of 320 nm, which gradually decreases as the emission wavelength moves beyond 325 nm.

In fact, the co-existence of oxygen and nitrogen-related functional groups on the surface layer and core structure have the ability to introduce their own discrete energy levels within the main energy gap, resulting in two additional recombination pathways besides band-to-band recombination.[71-74] However, based on XPS data showing a small amount of N-related functional groups in our sample compared to a larger proportion of O-related functional groups, it can be argued that

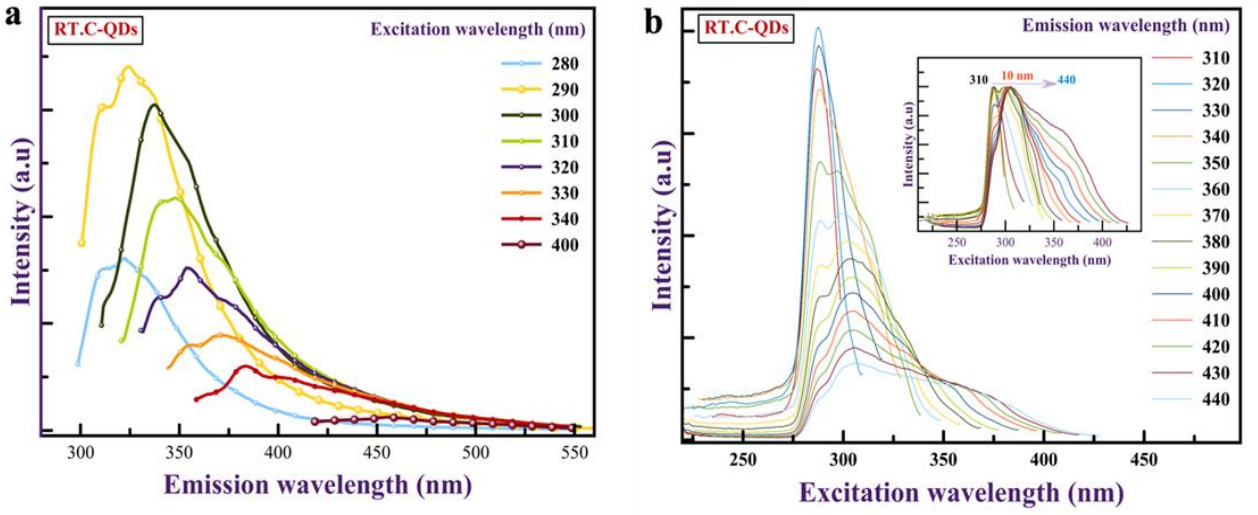

Fig. 11 (a) Photoluminescence spectra of RT.C-QDs at different excitation wavelengths. (b) PL excitation with emission wavelength variation from 310 to 440 nm (inset shows the normalization of the excitation spectra).

the influence of nitrogen on the PL is significantly smaller than the effect of O-related functional groups.

Combining all these characterization data, the proposed structural model and PL mechanism are presented in Fig. 12. Therefore, RT.C-QDs consist of a graphite core coated with an amorphous shell layer of oxygen and nitrogen-related functional groups. When electrons are excited at wavelengths between 280 and 290 nm, they can be deactivated by intersystem crossing (C-to-N, N-to-O) followed by vibrational relaxation and finally radiative recombination. In contrast, the energy required for π-π* transition cannot be accomplished with an excitation wavelength longer than 290 nm, and instead electrons are only excited to defect states within the bandgap and result in low-energy emission from the defect states.

5. Conclusions

In this study, we have successfully synthesized ambient temperature carbon quantum dots (RT.C-QDs) from Kakadu plum powder, opening a new avenue in the realm of nanotechnology. The meticulous investigation into the particle size and morphology through SEM and TEM analyses revealed a crystalline core structure with negligible defects, distinguishing these quantum dots from the predominantly reported amorphous carbon dots. The particles demonstrated a commendable size distribution, emphasizing their potential for varied applications.

Chemical composition analyses via XPS and FTIR have divulged critical information on the surface layer and core structure of the RT.C-QDs. These investigations underscored the prominence of carbon, nitrogen, and oxygen in the elemental composition, with a significant presence of functional groups such as OH, C=O, C-O/C-N, and C-H. This compositional richness paints a vivid picture of a graphite structure enveloped by amorphous shells, showcasing the

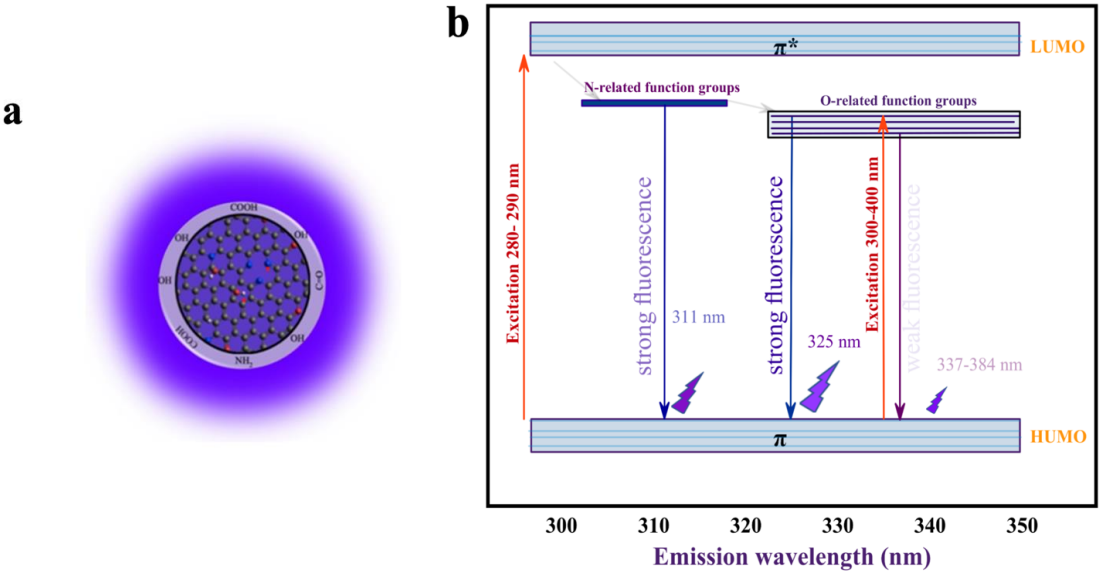

Fig. 12 (a) a schematic representation of the proposed structure of RT.C-QDs made of graphite core coated with an amorphous shell layer containing oxygen (red), nitrogen (blue) and hydrogen (white). (b) a proposed PL mechanism of excitation-dependent emission.

potential for further tuning and optimization of these quantum dots.

A striking feature of the synthesized RT.C-QDs is their high photostability, a prerequisite for numerous practical applications, including those requiring prolonged exposure to light. Their photoluminescence properties, sensitive to environmental factors like pH, exhibit stable emission peaks across a wide pH range, marking them as promising candidates for sensing applications.

Furthermore, this study unveils a promising structural model of RT.C-QDs, characterized by a graphite core coated with an amorphous shell layer, harboring oxygen and nitrogen-related functional groups. This structure engenders a complex yet insightful photoluminescence mechanism, offering a panorama of excitation-dependent emissions, which is pivotal in understanding the photophysics of these quantum dots.

In conclusion, this research stands as a beacon in the ongoing exploration of carbon quantum dots, shedding light on their synthesis from natural precursors and revealing intricate details of their structure and properties. The findings pave the way for further research, focusing on optimizing the synthesis process to fully carbonize the hydrocarbon components and exploring the vast application potential of these quantum dots, ranging from sensing to bio-imaging applications. The study thus holds the promise of steering the domain of nanotechnology towards a future replete with innovations, leveraging the unique properties of RT.C-QDs for groundbreaking developments.

We propose further studies to delve deeper into understanding the influence of various functional groups on the photoluminescence properties and exploring avenues for enhancing the performance and applicability of RT.C-QDs in real-world scenarios. Thus, this research not only contributes significantly to the existing body of knowledge but also shows the seeds for future groundbreaking discoveries in the fascinating world of nanotechnology.

Conflict of Interest

There is no conflict of interest.

Supporting Information

Applicable.

References

[1] S. W. Thomas, G. D. Joly, T. M. Swager, Chemical sensors based on amplifying fluorescent conjugated polymers, *Chemical Reviews*, 2007, **107**, 1339-1386, doi: 10.1021/cr0501339.

[2] Z. Guo, S. Park, J. Yoon, I. Shin, Recent progress in the development of near-infrared fluorescent probes for bioimaging applications, *Chemical Society Reviews*, 2014, **43**, 16-29, doi: 10.1039/c3cs60271k.

[3] O. S. Wolfbeis, An overview of nanoparticles commonly used in fluorescent bioimaging, *Chemical Society Reviews*, 2015, **44**, 4743-4768, doi: 10.1039/c4cs00392f.

[4] J. Mei, N. L. C. Leung, R. T. K. Kwok, J. W. Y. Lam, B. Z. Tang, Aggregation-induced emission: together we shine, united we soar!, *Chemical Reviews*, 2015, **115**, 11718-11940, doi: 10.1021/acs.chemrev.5b00263.

[5] J. M. Pietryga, Y.-S. Park, J. Lim, A. F. Fidler, W. K. Bae, S. Brovelli, V. I. Klimov, Spectroscopic and device aspects of nanocrystal quantum dots, *Chemical Reviews*, 2016, **116**, 10513-10622, doi: 10.1021/acs.chemrev.6b00169.

[6] Y. Liu, C. Li, Z. Ren, S. Yan, M. R. Bryce, All-organic thermally activated delayed fluorescence materials for organic light-emitting diodes, *Nature Reviews Materials*, 2018, **3**, 18020, doi: 10.1038/natrevmats.2018.20.

[7] L. N. Quan, F. P. G. de Arquer, R. P. Sabatini, E. H. Sargent, Perovskites for light emission, *Advanced Materials*, 2018, **30**, 1801996, doi: 10.1002/adma.201801996.

[8] J. You, X. Zhang, Q. Nan, K. Jin, J. Zhang, Y. Wang, C. Yin, Z. Yang, J. Zhang, Aggregation-regulated room-temperature phosphorescence materials with multi-mode emission, adjustable excitation-dependence and visible-light excitation, *Nature Communications*, 2023, **14**, 4163, doi: 10.1038/s41467-023-39767-w.

[9] M. Kurian, A. Paul, Recent trends in the use of green sources for carbon dot synthesis-a short review, *Carbon Trends*, 2021, **3**, 100032, doi: 10.1016/j.cartre.2021.100032.

[10] J. R. Bhamore, S. Jha, T. J. Park, S. K. Kailasa, Green synthesis of multi-color emissive carbon dots from Manilkara zapota fruits for bioimaging of bacterial and fungal cells, *Journal of Photochemistry and Photobiology B: Biology*, 2019, **191**, 150-155, doi: 10.1016/j.jphotobiol.2018.12.023.

[11] H. Li, Z. Kang, Y. Liu, S.-T. Lee, Carbon nanodots: synthesis, properties and applications, *Journal of Materials Chemistry*, 2012, **22**, 24230, doi: 10.1039/c2jm34690g.

[12] X. Wang, Y. Feng, P. Dong, J. Huang, A mini review on carbon quantum dots: preparation, properties, and electrocatalytic application, *Frontiers in Chemistry*, 2019, **7**, 671, doi: 10.3389/fchem.2019.00671.

[13] L. Cui, X. Ren, M. Sun, H. Liu, L. Xia, Carbon dots: synthesis, properties and applications, *Nanomaterials*, 2021, **11**, 3419, doi: 10.3390/nano11123419.

[14] X. Ma, Y. Dong, H. Sun, N. Chen, Highly fluorescent carbon dots from peanut shells as potential probes for copper ion: the optimization and analysis of the synthetic process, *Materials Today Chemistry*, 2017, **5**, 1-10, doi: 10.1016/j.mtchem.2017.04.004.

[15] X. Xu, R. Ray, Y. Gu, H. J. Ploehn, L. Gearheart, K. Raker, W. A. Scrivens, Electrophoretic analysis and purification of fluorescent single-walled carbon nanotube fragments, *Journal of the American Chemical Society*, 2004, **126**, 12736-12737, doi: 10.1021/ja040082h.

[16] H. Ding, S.-B. Yu, J.-S. Wei, H.-M. Xiong, Full-color light-emitting carbon dots with a surface-state-controlled luminescence mechanism, *ACS Nano*, 2016, **10**, 484-491, doi: 10.1021/acsnano.5b05406.

[17] F. Yuan, Z. Wang, X. Li, Y. Li, Z.-A. Tan, L. Fan, S. Yang, Bright multicolor bandgap fluorescent carbon quantum dots for

electroluminescent light-emitting diodes, *Advanced Materials*, 2017, **29**, 1604436, doi: 10.1002/adma.201604436.
[18] L. Wang, W. Li, L. Yin, Y. Liu, H. Guo, J. Lai, Y. Han, G. Li, M. Li, J. Zhang, R. Vajtai, P. M. Ajayan, M. Wu, Full-color fluorescent carbon quantum dots, *Science Advances*, 2020, **6**, eabb6772, doi: 10.1126/sciadv.abb6772.
[19] N. K. Khairol Anuar, H. L. Tan, Y. P. Lim, M. S. So'aib, N. F. Abu Bakar, A review on multifunctional carbon-dots synthesized from biomass waste: design/fabrication, characterization and applications, *Frontiers in Energy Research*, 2021, **9**, 626549, doi: 10.3389/fenrg.2021.626549.
[20] M. Semeniuk, Z. Yi, V. Poursorkhabi, J. Tjong, S. Jaffer, Z.-H. Lu, M. Sain, Future perspectives and review on organic carbon dots in electronic applications, *ACS Nano*, 2019, **13**, 6224-6255, doi: 10.1021/acsnano.9b00688.
[21] R. B. González-González, L. Teresa González, M. Madou, C. Leyva-Porras, S. O. Martinez-Chapa, A. Mendoza, Synthesis, purification, and characterization of carbon dots from non-activated and activated pyrolytic carbon black, *Nanomaterials*, 2022, **12**, 298, doi: 10.3390/nano12030298.
[22] B. Zhi, X. Yao, M. Wu, A. Mensch, Y. Cui, J. Deng, J. J. Duchimaza-Heredia, K. J. Trerayapiwat, T. Niehaus, Y. Nishimoto, B. P. Frank, Y. Zhang, R. E. Lewis, E. A. Kappel, R. J. Hamers, H. D. Fairbrother, G. Orr, C. J. Murphy, Q. Cui, C. L. Haynes, Multicolor polymeric carbon dots: synthesis, separation and polyamide-supported molecular fluorescence, *Chemical Science*, 2021, **12**, 2441-2455, doi: 10.1039/d0sc05743f.
[23] C. Xia, S. Zhu, T. Feng, M. Yang, B. Yang, Evolution and synthesis of carbon dots: from carbon dots to carbonized polymer dots, *Advanced Science*, 2019, **6**, 1901316, doi: 10.1002/advs.201901316.
[24] S. Sugiarti, N. Darmawan, Synthesis of fluorescence carbon nanoparticles from ascorbic acid, *Indonesian Journal of Chemistry*, 2015, **15**, 141-145, doi: 10.22146/ijc.21207.
[25] H. Wu, C. Mi, H. Huang, B. Han, J. Li, S. Xu, Solvothermal synthesis of green-fluorescent carbon nanoparticles and their application, *Journal of Luminescence*, 2012, **132**, 1603-1607, doi: 10.1016/j.jlumin.2011.12.077.
[26] Q. Li, T. Y. Ohulchanskyy, R. Liu, K. Koynov, D. Wu, A. Best, R. Kumar, A. Bonoiu, P. N. Prasad, Photoluminescent carbon dots as biocompatible nanoprobes for targeting cancer cells *in vitro*, *The Journal of Physical Chemistry C*, 2010, **114**, 12062-12068, doi: 10.1021/jp911539r.
[27] M. Langer, M. Paloncýová, M. Medveď, M. Pykal, D. Nachtigallová, B. Shi, A. J. A. Aquino, H. Lischka, M. Otyepka, Progress and challenges in understanding of photoluminescence properties of carbon dots based on theoretical computations, *Applied Materials Today*, 2021, **22**, 100924, doi: 10.1016/j.apmt.2020.100924.
[28] S. Zhu, Y. Song, X. Zhao, J. Shao, J. Zhang, B. Yang, The photoluminescence mechanism in carbon dots (graphene quantum dots, carbon nanodots, and polymer dots): current state and future perspective, *Nano Research*, 2015, **8**, 355-381, doi: 10.1007/s12274-014-0644-3.
[29] M. Liu, Optical properties of carbon dots: a review, *Nanoarchitectonics*, 2020, **1**, 1-12, doi: 10.37256/nat.112020124.1-12.
[30] X.-T. Tian, X.-B. Yin, Carbon dots, unconventional preparation strategies, and applications beyond photoluminescence, *Small*, 2019, **15**, 1901803, doi: 10.1002/smll.201901803.
[31] F. Yan, Z. Sun, H. Zhang, X. Sun, Y. Jiang, Z. Bai, The fluorescence mechanism of carbon dots, and methods for tuning their emission color: a review, *Microchimica Acta*, 2019, **186**, 1-37, doi: 10.1007/s00604-019-3688-y.
[32] N. Azam, M. Najabat Ali, T. Javaid Khan, Carbon quantum dots for biomedical applications: review and analysis, *Frontiers in Materials*, 2021, **8**, 700403, doi: 10.3389/fmats.2021.700403.
[33] B. D. Mansuriya, Z. Altintas, Carbon dots: classification, properties, synthesis, characterization, and applications in health care-an updated review (2018-2021), *Nanomaterials*, 2021, **11**, 2525, doi: 10.3390/nano11102525.
[34] B. Vercelli, The role of carbon quantum dots in organic photovoltaics: a short overview, *Coatings*, 2021, **11**, 232, doi: 10.3390/coatings11020232.
[35] Y.-P. Sun, B. Zhou, Y. Lin, W. Wang, K. A. S. Fernando, P. Pathak, M. J. Meziani, B. A. Harruff, X. Wang, H. Wang, P. G. Luo, H. Yang, M. E. Kose, B. Chen, L. M. Veca, S.-Y. Xie, Quantum-sized carbon dots for bright and colorful photoluminescence, *Journal of the American Chemical Society*, 2006, **128**, 7756-7757, doi: 10.1021/ja062677d.
[36] L. Wang, W. M. Choi, J. S. Chung, S. H. Hur, Multicolor emitting N-doped carbon dots derived from ascorbic acid and phenylenediamine precursors, *Nanoscale Research Letters*, 2020, **15**, 1-10, doi: 10.1186/s11671-020-03453-3.
[37] A. Dager, A. Baliyan, S. Kurosu, T. Maekawa, M. Tachibana, Ultrafast synthesis of carbon quantum dots from fenugreek seeds using microwave plasma enhanced decomposition: application of C-QDs to grow fluorescent protein crystals, *Scientific Reports*, 2020, **10**, 12333, doi: 10.1038/s41598-020-69264-9.
[38] M. J. Krysmann, A. Kelarakis, P. Dallas, E. P. Giannelis, Formation mechanism of carbogenic nanoparticles with dual photoluminescence emission, *Journal of the American Chemical Society*, 2012, **134**, 747-750, doi: 10.1021/ja204661r.
[39] B. B. Chen, Z. X. Liu, W. C. Deng, L. Zhan, M. L. Liu, C. Z. Huang, A large-scale synthesis of photoluminescent carbon quantum dots: a self-exothermic reaction driving the formation of the nanocrystalline core at room temperature, *Green Chemistry*, 2016, **18**, 5127-5132, doi: 10.1039/c6gc01820c.
[40] J. Zhang, W. Shen, D. Pan, Z. Zhang, Y. Fang, M. Wu, Controlled synthesis of green and blue luminescent carbon nanoparticles with high yields by the carbonization of sucrose, *New Journal of Chemistry*, 2010, **34**, 591, doi: 10.1039/b9nj00662a.
[41] S. Mitra, S. Chandra, S. H. Pathan, N. Sikdar, P. Pramanik, A. Goswami, Room temperature and solvothermal green synthesis of self passivated carbon quantum dots, *RSC Advances*, 2013, **3**, 3189, doi: 10.1039/c2ra23085b.
[42] J. Zhang, W. Shen, D. Pan, Z. Zhang, Y. Fang, M. Wu, Controlled synthesis of green and blue luminescent carbon

nanoparticles with high yields by the carbonization of sucrose, *New Journal of Chemistry*, 2010, **34**, 591, doi: 10.1039/b9nj00662a.
[43] S. J. Xiao, Z. J. Chu, J. Zuo, X. J. Zhao, C. Z. Huang, L. Zhang, Fluorescent carbon dots: facile synthesis at room temperature and its application for Fe^{2+} sensing, *Journal of Nanoparticle Research*, 2017, **19**, 1-8, doi: 10.1007/s11051-016-3698-1.
[44] Y. Huang, X. Huang, H. Lin, Z. Liu, Y. Zong, Room temperature driven highly crystalline fluorine-doped carbon quantum dots for sensitive tetracycline sensing, *Optical Materials*, 2021, **114**, 110967, doi: 10.1016/j.optmat.2021.110967.
[45] C. Kang, Y. Huang, H. Yang, X. F. Yan, Z. P. Chen, A review of carbon dots produced from biomass wastes, *Nanomaterials*, 2020, **10**, 2316, doi: 10.3390/nano10112316.
[46] S. Zhu, Q. Meng, L. Wang, J. Zhang, Y. Song, H. Jin, K. Zhang, H. Sun, H. Wang, B. Yang, Highly photoluminescent carbon dots for multicolor patterning, sensors, and bioimaging, *Angewandte Chemie International Edition*, 2013, **52**, 3953-3957, doi: 10.1002/anie.201300519.
[47] K. Jiang, S. Sun, L. Zhang, Y. Lu, A. Wu, C. Cai, H. Lin, Red, green, and blue luminescence by carbon dots: full-color emission tuning and multicolor cellular imaging, *Angewandte Chemie International Edition*, 2015, **54**, 5360-5363, doi: 10.1002/anie.201501193.
[48] C. Cheng, Y. Shi, M. Li, M. Xing, Q. Wu, Carbon quantum dots from carbonized walnut shells: structural evolution, fluorescence characteristics, and intracellular bioimaging, *Materials Science and Engineering: C*, 2017, **79**, 473-480, doi: 10.1016/j.msec.2017.05.094.
[49] S. Zhao, M. Lan, X. Zhu, H. Xue, T.-W. Ng, X. Meng, C.-S. Lee, P. Wang, W. Zhang, Green synthesis of bifunctional fluorescent carbon dots from garlic for cellular imaging and free radical scavenging, *ACS Applied Materials & Interfaces*, 2015, **7**, 17054-17060, doi: 10.1021/acsami.5b03228.
[50] B. S. B. Kasibabu, S. L. D'souza, S. Jha, S. K. Kailasa, Imaging of bacterial and fungal cells using fluorescent carbon dots prepared from carica papaya juice, *Journal of Fluorescence*, 2015, **25**, 803-810, doi: 10.1007/s10895-015-1595-0.
[51] Z. Wang, J. Yu, X. Zhang, N. Li, B. Liu, Y. Li, Y. Wang, W. Wang, Y. Li, L. Zhang, S. Dissanayake, S. L. Suib, L. Sun, Large-scale and controllable synthesis of graphene quantum dots from rice husk biomass: a comprehensive utilization strategy, *ACS Applied Materials & Interfaces*, 2016, **8**, 1434-1439, doi: 10.1021/acsami.5b10660.
[52] Xie, Cheng, Liu, Han, Green hydrothermal synthesis of N-doped carbon dots from biomass highland barley for the detection of Hg^{2+}, *Sensors*, 2019, **19**, 3169, doi: 10.3390/s19143169.
[53] M. Xue, M. Zou, J. Zhao, Z. Zhan, S. Zhao, Green preparation of fluorescent carbon dots from lychee seeds and their application for the selective detection of methylene blue and imaging in living cells, *Journal of Materials Chemistry B*, 2015, **3**, 6783-6789, doi: 10.1039/c5tb01073j.
[54] H. Jing, F. Bardakci, S. Akgöl, K. Kusat, M. Adnan, M. Alam, R. Gupta, S. Sahreen, Y. Chen, S. Gopinath, S. Sasidharan, Green carbon dots: synthesis, characterization, properties and biomedical applications, *Journal of Functional Biomaterials*, 2023, **14**, 27, doi: 10.3390/jfb14010027.
[55] S. K. Tiwari, M. Bystrzejewski, A. De Adhikari, A. Huczko, N. Wang, Methods for the conversion of biomass waste into value-added carbon nanomaterials: recent progress and applications, *Progress in Energy and Combustion Science*, 2022, **92**, 101023, doi: 10.1016/j.pecs.2022.101023.
[56] H. Jia, Z. Wang, T. Yuan, F. Yuan, X. Li, Y. Li, Z.-A. Tan, L. Fan, S. Yang, Electroluminescent warm white light-emitting diodes based on passivation enabled bright red bandgap emission carbon quantum dots, *Advanced Science*, 2019, **6**, 1900397, doi: 10.1002/advs.201900397.
[57] F. Arcudi, L. Đorđević, M. Prato, Rationally designed carbon nanodots towards pure white-light emission, *Angewandte Chemie International Edition*, 2017, **56**, 4170-4173, doi: 10.1002/anie.201612160.
[58] M. Gore, Spectrophotometry and Spectrofluorimetry, OUP Oxford, 2000.
[59] K. W. Yong, D. Yuen, M. Z. Chen, C. J. H. Porter, A. P. R. Johnston, Pointing in the right direction: controlling the orientation of proteins on nanoparticles improves targeting efficiency, *Nano Letters*, 2019, **19**, 1827-1831, doi: 10.1021/acs.nanolett.8b04916.
[60] A. B. Siddique, A. K. Pramanick, S. Chatterjee, M. Ray, Amorphous carbon dots and their remarkable ability to detect 2, 4, 6-trinitrophenol, *Scientific Reports*, 2018, **8**, 9770, doi: 10.1038/s41598-018-28021-9.
[61] G. Tong, J. Wang, R. Wang, X. Guo, L. He, F. Qiu, G. Wang, B. Zhu, X. Zhu, T. Liu, Amorphous carbon dots with high two-photon fluorescence for cellular imaging passivated by hyperbranched poly(amino amine), *Journal of Materials Chemistry B*, 2015, **3**, 700-706, doi: 10.1039/c4tb01643b.
[62] X. Liu, J. Pang, F. Xu, X. Zhang, Simple approach to synthesize amino-functionalized carbon dots by carbonization of chitosan, *Scientific Reports*, 2016, **6**, 31100, doi: 10.1038/srep31100.
[63] D. Pan, J. Zhang, Z. Li, M. Wu, Hydrothermal route for cutting graphene sheets into blue-luminescent graphene quantum dots, *Advanced Materials*, 2010, **22**, 734-738, doi: 10.1002/adma.200902825.
[64] Y. Zhang, A. Ye, Y. Yao, C. Yao, A sensitive near-infrared fluorescent probe for detecting heavy metal Ag+ in water samples, *Sensors*, 2019, **19**, 247, doi: 10.3390/s19020247.
[65] Y. Wang, A. Hu, Carbon quantum dots: synthesis, properties and applications, *Journal of Materials Chemistry C*, 2014, **2**, 6921, doi: 10.1039/c4tc00988f.
[66] M. Sudolská, M. Dubecký, S. Sarkar, C. J. Reckmeier, R. Zbořil, A. L. Rogach, M. Otyepka, Nature of absorption bands in oxygen-functionalized graphitic carbon dots, *The Journal of Physical Chemistry C*, 2015, **119**, 13369-13373, doi: 10.1021/acs.jpcc.5b04080.
[67] J. Zhu, X. Bai, J. Bai, G. Pan, Y. Zhu, Y. Zhai, H. Shao, X. Chen, B. Dong, H. Zhang, H. Song, Emitting color tunable carbon

dots by adjusting solvent towards light-emitting devices, *Nanotechnology*, 2018, **29**, 085705, doi: 10.1088/1361-6528/aaa321.
[68] Z. Gan, H. Xu, Y. Hao, Mechanism for excitation-dependent photoluminescence from graphene quantum dots and other graphene oxide derivates: consensus, debates and challenges, *Nanoscale*, 2016, **8**, 7794-7807, doi: 10.1039/c6nr00605a.
[69] Y. Xiong, J. Schneider, E. V. Ushakova, A. L. Rogach, Influence of molecular fluorophores on the research field of chemically synthesized carbon dots, *Nano Today*, 2018, **23**, 124-139, doi: 10.1016/j.nantod.2018.10.010.
[70] A. Sharma, T. Gadly, A. Gupta, A. Ballal, S. K. Ghosh, M. Kumbhakar, Origin of excitation dependent fluorescence in carbon nanodots, *The Journal of Physical Chemistry Letters*, 2016, **7**, 3695-3702, doi: 10.1021/acs.jpclett.6b01791.
[71] K. Holá, M. Sudolská, S. Kalytchuk, D. Nachtigallová, A. L. Rogach, M. Otyepka, R. Zbořil, Graphitic nitrogen triggers red fluorescence in carbon dots, *ACS Nano*, 2017, **11**, 12402-12410, doi: 10.1021/acsnano.7b06399.
[72] H. Liu, Z. He, L.-P. Jiang, J.-J. Zhu, Microwave-assisted synthesis of wavelength-tunable photoluminescent carbon nanodots and their potential applications, *ACS Applied Materials & Interfaces*, 2015, **7**, 4913-4920, doi: 10.1021/am508994w.
[73] L. Bao, Z.-L. Zhang, Z.-Q. Tian, L. Zhang, C. Liu, Y. Lin, B. Qi, D.-W. Pang, Electrochemical tuning of luminescent carbon nanodots: from preparation to luminescence mechanism, *Advanced Materials*, 2011, **23**, 5801-5806, doi: 10.1002/adma.201102866.
[74] L. Tang, R. Ji, X. Li, K. S. Teng, S. P. Lau, Energy-level structure of nitrogen-doped graphene quantum dots, *Journal of Materials Chemistry C*, 2013, **1**, 4908, doi: 10.1039/c3tc30877d.

